Journal of Aerosol Science 62 (2013) 15–25

Contents lists available at SciVerse ScienceDirect

Journal of Aerosol Science

journal homepage: www.elsevier.com/locate/jaerosci

Shear stress and particle removal measurements of a round turbulent air jet impinging normally upon a planar wall

R.M. Young *, M.J. Hargather, G.S. Settles

Penn State Gas Dynamics Laboratory, 301D Reber Building, University Park, PA, 16802, USA

ARTICLE INFO

Article history:
Received 2 July 2012
Received in revised form
2 April 2013
Accepted 2 April 2013
Available online 11 April 2013

Keywords:
Oil-film interferometry
Shear stress
Particle removal
Air jet

ABSTRACT

When a round jet of air impinges normally upon a wall, it imposes a shear stress parallel to the wall in all directions from the impingement point. Particle removal from that surface is assumed to be mainly due to the imposed shear stress. This shear stress has been difficult to measure directly and has, in the past, been inferred from particle removal rates. Here we make a fundamental measurement of the mean shear stress imposed upon a planar wall by a normally-impinging turbulent air jet using the technique of oil-film interferometry. The resulting shear–stress distribution is then compared with measured removal rates of latex microspheres from a planar glass surface as a function of the radial distance from jet impingement normalized by the height of the nozzle exit above the surface. The particle removal experiments are carried out with sparse (few collisions) particle distributions. These experiments show that the efficiency of particle removal is directly but not linearly related to the imposed shear stress. A distinct shear stress threshold was found, below which little or no particle removal occurred.

1. Introduction

Many studies have been performed on the removal or resuspension of particles in a turbulent flow. Reviews by Ziskind et al. (1995, 2006) and Nicholson (1988) attempt to synthesize an overall perspective from these many varied contributions. Fromentin (1989), for example, removed particles from a plate in a wind tunnel, where removal was measured as a resuspended mass flux per unit time and unit surface area. Ibrahim et al. (2003) performed a study in which microspheres were removed from a smooth glass surface during an accelerating turbulent flow caused by wind-tunnel startup. Their results indicate that the surface energy of adhesion and the microsphere radius are the primary factors in particle removal. Braaten et al. (1990) also performed several experiments in a wind tunnel, and concluded that particles were removed based on discrete events such as velocity fluctuations or “bursts” within the boundary layer. Such bursts were earlier described by Corino & Brodkey (1969).

Early studies of particle resuspension resulted in a traditional aerodynamic model of the process. Initially, a lift force related to the imposed aerodynamic shear stress was thought to act against the combined forces of particle adhesion to a surface. When adhesion is overcome, resuspension of the particle occurs. This traditional force-balance view has been modified by investigators such as Reeks et al. (1988), who saw particles accumulating energy from turbulent fluctuations of the resuspending airflow. Resuspension occurs when a particle accumulates enough vibratory energy to escape from the “potential well” of surface adhesion.

* Corresponding author. Tel.: +1 610 724 9473.
E-mail addresses: rmy5009@psu.edu (R.M. Young), mjh340@psu.edu (M.J. Hargather), gss2@psu.edu (G.S. Settles).

0021-8502/$ - see front matter © 2013 Elsevier Ltd. All rights reserved.
http://dx.doi.org/10.1016/j.jaerosci.2013.04.002

Nomenclature

D	nozzle diameter, mm
H	jet standoff distance, mm
h	oil thickness, μm
N	fringe number from leading edge
N_{after}	number of particles after shear stress is applied
N_{before}	number of particles before shear stress is applied
n_a	refractive index of air
n_o	refractive index of oil
r	radial distance from jet impingement point, mm
r_0	radial distance from jet impingement point to leading edge of oil-film, mm
P_{atm}	atmospheric pressure, kPa
P_{jet}	Jet exit pressure, kPa
Re_o	Reynolds number at jet exit based on exit diameter
t	duration of jet impingement, s
u_o	average jet exit velocity, m/s
θ_i	light incidence angle, degrees
λ	wavelength of illumination, nm
μ_o	viscosity of oil, Pa s
ρ_a	density of air, kg/m^3
τ	shear stress, Pa
τ_{cr}	critical shear stress, Pa
τ_{max}	theoretical/experimental maximum shear stress, Pa

More recently, Ziskind et al. (1997) showed that a hydrodynamic moment is associated with particle adhesion to a surface, leading to particle rotation which plays a role in detachment. Reeks & Hall (2001) then proposed a *rock'n roll* model of particle detachment: instead of leaping from the surface into the surrounding fluid due to a lift force, particles can rock or rotate about their attachment points until they eventually roll off along the surface in the downwind direction. This view of particle resuspension physics is now widely accepted.

Also pertinent to the present study are a few recent studies of particle resuspension due to impact by a particle rolling along the surface from upstream, John et al. (1991) and Ibrahim et al. (2004), also reviewed by Ziskind (2006). It is clear from these studies that such particle impacts, when they occur, contribute to resuspension by a mechanism that is in addition to the single-particle resuspension physics described above.

A subset of the general resuspension literature is devoted to a turbulent gas jet impinging upon a particle-laden surface. This special case has applications in microelectronics manufacturing, homeland security, etc. Smedley et al. (2001) and Ziskind et al. (2002) examined the case of jet impingement at an angle less than 90°. The latter study involved pulsed jets, where it was found that resuspension depends upon the pulsing frequency. An analogy was drawn between particle removal and surface cooling due to pulsed jet impingement.

Smedley et al., 1999 and Phares et al., 2000, used a normally-impinging round airjet upon a glass plate to measure the removal rates of monodisperse particles. The shear–stress profile thus produced was inferred by analyzing these removal rates, thus introducing the idea that such particles could behave as shear–stress sensors. By knowing the jet standoff distance, nozzle diameter, and $P_{\text{jet}}/P_{\text{atm}}$, and by determining the size of the particle removal path created by sweeping a normally-impinging jet over a uniform particle distribution, these authors estimated the aerodynamic shear–stress profile due to jet impingement. However, this technique assumes that the imposed shear stress is directly responsible for resuspension, and it is unable to account for the influence of particle impacts in dense particle distributions.

Based on this literature we make two observations which motivate our present contribution to this topic:

1) In many cases, resuspension experiments were done in uniform wind-tunnel-like flows where the aerodynamic shear stress τ imposed upon the surface was known or easily determined. Only a few studies (John, 1991; Smedley et al., 1999; Phares et al., 2000; Smedley et al., 2001; Ziskind et al., 2002) considered resuspension due to gas-jet impingement upon a particle-bearing surface. The imposed shear–stress distribution in this case is not yet well-defined in our opinion.
2) The majority of published resuspension experiments took no account of the density of particles applied to surfaces prior to testing, or of the potential for impact-induced resuspension by particles rolling along the surface. (Exceptions include Braaten (1994) and Ibrahim et al. (2003, 2004, 2006, 2008), who tested near the leading edge of deposited particles in order to eliminate particle impacts from upstream). Resuspension modeling, on the other hand, generally considers the case of individual particles rather than particle distributions, and especially not dense distributions. There apparently exists no definition of what constitutes a sparse vs. a dense particle distribution in this regard.

With these observations in mind, the goals of the present research are to measure the mean surface shear–stress profile of a normally-impinging axisymmetric air jet from first principles using the oil-film interferometry technique, and to correlate these data in terms of a non-dimensional shear stress profile. Then, we utilize the knowledge of this profile to explore the effect of the initial particle distribution density upon particle removal efficiency. Finally a sparse particle distribution – wherein particles react to the applied aerodynamic shear stress independently of other particles – is used to examine the resuspension rate as a function of the aerodynamic shear stress.

2. Shear stress measurements

2.1. Experimental methods

2.1.1. Oil-film interferometry

Oil-film interferometry (OFI) is an experimental method that utilizes the optical fringe pattern in a very-thin film of oil to determine mean wall shear stress. The shear stress at each interference fringe location can be derived from the measured slope of the oil film. Tanner & Blows (1976) were the first to derive the theory of shear stress measurement from oil fringe patterns, while Driver (2003) and Naughton (2005) further developed this technique toward its present state of refinement for high-quality measurements of shear stress.

The experimental OFI setup used here is shown schematically in Fig. 1a. A sodium-ion arc lamp with two distinct wavelengths of 589 and 589.6 nm was the illumination source. The light was diffused by ground glass to provide uniform illumination, and was directed with a 60° angle of incidence, θ_i, to the test surface.

The shear stress measurements were performed on a 0.25 cm thick by 25 cm square polished glass plate test surface. Dow Corning 200 Fluid ($\mu_o = 50$ cs at 25 °C) was chosen for the oil film because of its ability to maintain a consistent viscosity at varying temperatures. The oil temperature was held at 22.5 °C ± 2.5 °C, corresponding to an average oil viscosity of 51 ± 1 cs. Thus, the oil viscosity remained within ± 2% for all present experiments.

A compressed-air cylinder with a flow regulator fed dry air to a straight tubular nozzle ($D = 3.75$ mm) to produce the impinging jet. A Nikon D80 digital SLR camera captured still images of the oil-film experiments at 12 megapixel resolution.

2.1.2. Impinging jet setup

Round free jets, such as those produced here, are considered to have fully-developed velocity profiles at a distance of 8 nozzle diameters downstream of the nozzle exit (Phares et al., 2000). For the present study, only fully-developed round jet impingements were considered, and the minimum standoff distance (distance from nozzle exit to plate surface) for these experiments was determined accordingly. The standoff distance was thus varied between 6 cm ($H/D = 16$) and 7.5 cm ($H/D = 20$) for these tests. A straight-walled tubular nozzle was used, as shown in Fig. 1b.

The jet stagnation pressure was varied independently using a pressure regulator attached to the compressed air source. Data were recorded for both subsonic and sonic jet exit conditions. A plenum chamber was used in order to stabilize the stagnation pressure during each test. This resulted in a variation of no more than ± 3.4 kPa. The subsonic data were taken

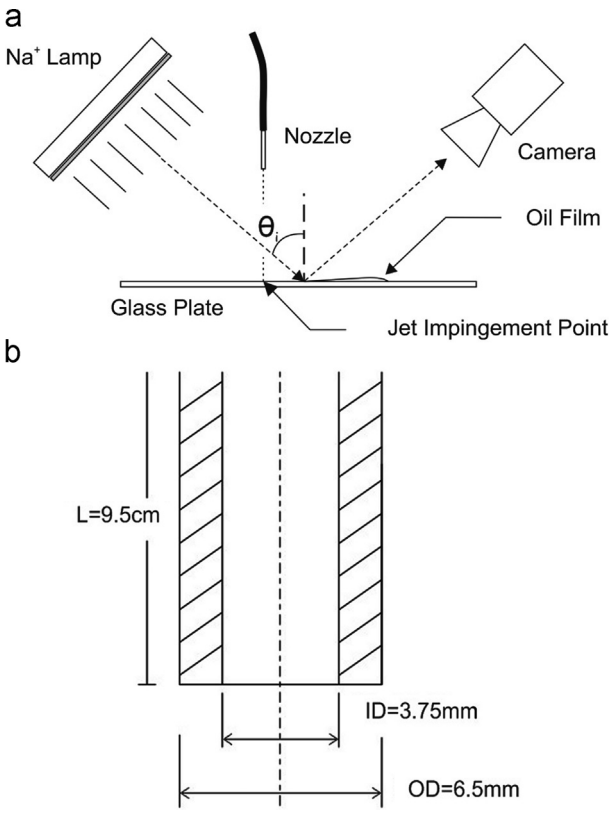

Fig. 1. (a) Schematic of the OFI setup and (b) straight nozzle dimensions.

with a stagnation pressure ratio P_{jet}/P_{atm} of 1.11 ± 0.04, which yielded an average exit velocity of 136 m/s and an exit Reynolds number (Re_o) of 3.3×10^4 for an air temperature of 296 K. Sonic-nozzle-exit data were taken with $P_{jet}/P_{atm}=2.52 \pm 0.04$, which produced underexpanded flow and shock diamonds just after the flow exited the nozzle.

2.1.3. Oil-film-interferometry imaging and processing

A calibration image is recorded for each experiment to convert pixel dimensions to radial distances. Each test begins by placing a drop of oil on the glass at the jet impingement point. The air jet is then turned on and is run continuously until a clear interference fringe pattern forms around the impingement point, as shown in Fig. 2. An image is taken of this pattern and it is processed to determine the pixel value of the ring center, which is the jet impingement point ($r=0$). The glass is then cleaned and an oil-film with a straight leading edge is placed beside the impingement point. This oil-film is created by first placing a drop of oil on the glass, then smearing the oil with a razor blade, thus providing an approximately-zero oil thickness at the film leading edge. (The location of zero oil thickness is required to subsequently determine the oil thickness at each of the fringe locations.) The air jet is then turned on continuously and an image of the oil-film interference pattern on the glass is taken every 10 s. Fig. 3a shows a typical image of the interference pattern in the oil-film with a straight leading edge at the left.

Each recorded image is converted to grayscale and a plot of pixel intensity versus pixel number along the radius of the jet impingement is obtained using MATLAB (Fig. 3b). Each maximum and minimum in Fig. 3b marks the center of a bright fringe and a dark fringe, respectively. The height of the oil at each of these points can be determined according to Naughton & Liu (2007) using

$$h = \frac{N\lambda}{4}\left(\frac{1}{\sqrt{n_o^2 - n_a^2 \sin^2\theta_i}}\right) \tag{1}$$

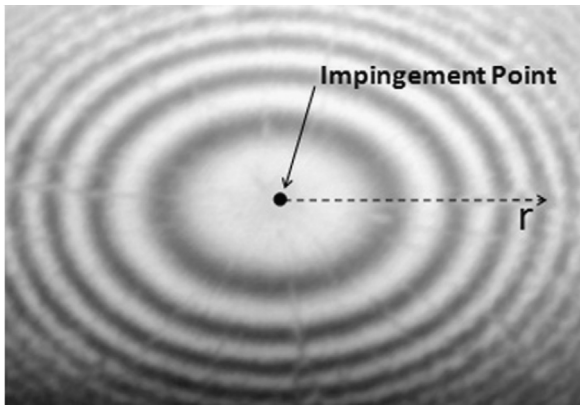

Fig. 2. Concentric interference fringes observed when oil drop is placed at impingement point.

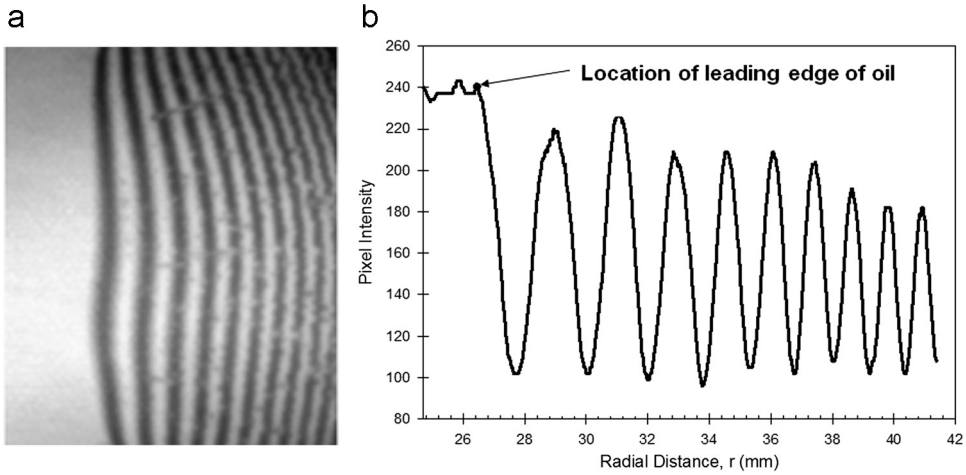

Fig. 3. (a) Fringe pattern in oil with a straight leading edge and (b) pixel intensity vs. radial distance from impingement point.

knowing the oil height h at each fringe location allows it to be expressed as a function of the radial distance (r) from the impingement point. The shear stress can then be found according to Tanner & Blows (1976),

$$\tau = \frac{2\mu_o}{th^2 r}\int_{r_0}^{r} hrdr \tag{2}$$

The calculation of τ is performed at each fringe location, integrating from r_0 to the radial distance, r, of the fringe in question.

2.2. Experimental results

The first experiments were performed with a pressure ratio (P_{jet}/P_{atm}) of 1.11 ± 0.04, yielding a subsonic average nozzle exit velocity of 136 m/s. The shear stress profile was first determined for a jet standoff distance of 7.5 cm ($H/D=20$) using the procedure described in Section 2.1. The jet standoff distance was then decreased to 6 cm ($H/D=16$) for the same jet exit condition, which increased the maximum shear stress at the surface by about 15%. The measured shear stress as a function of radial distance from jet impingement for both of these nozzle standoff heights is plotted in Fig. 4.

The data of Fig. 4 can be non-dimensionalized to allow comparisons between experiments: the radial distance is normalized as r/H, and the shear stress is normalized as τ/τ_{max}, where τ_{max} is the theoretical maximum shear stress, which occurs at $r/H=0.09$ as found by Phares et al. (2000)

$$\tau_{max} = 44.6\rho u_o^2 Re_0^{-1/2}\left(\frac{H}{D}\right)^{-2} \tag{3}$$

The normalized data from Fig. 4 are plotted in Fig. 5, where it is observed that the normalization succeeds in collapsing the effect of varying nozzle standoff distance.

The present experimental results were compared to theoretical laminar boundary layer impingement-region behavior and the experimental results of Smedley et al. (1999), as shown in Figs. 6a and b. A laminar impingement region is used here, as also used by Smedley et al. (1999), because it was assumed that the strong favorable pressure gradient in the impingement region will cause the turbulent jet flow to re-laminarize. However, this assumption was not previously supported by observation. Based on a subsonic exit flow with a jet spreading half-angle of 12° (Pope, 2000), the jet-impingement region ends at an r/H of 0.21 in Figs. 6a and b. The experimental results match the predicted shear stress from laminar-boundary-layer impingement-region theory quite well for $0 < r/H < 0.21$. This also appears to be the location beyond which the data from Smedley et al. (1999) no longer match the present OFI results in Fig. 6a.

The comparison in Fig. 6a between the present results and those of Smedley et al. (1999) is an important one that bears discussion. Smedley et al. assumed that the impinging-jet wall shear stress distribution could be directly inferred from their measured particle removal data, whereas we have measured the mean wall shear stress directly without reference to particle removal. The similar behavior of the two datasets, revealed in Fig. 6a, indeed supports the widely-assumed traditional model of particle removal due to aerodynamic drag, but the comparison is not perfect. Outside the immediate jet-impingement zone, i.e. for $r/H > 0.21$, the present shear–stress data rapidly asymptote toward zero whilst the shear–stress-inferred-from-particle-removal data of Smedley et al. (1999) remain distinctly higher. The reason for this discrepancy is not known, but two important differences in the datasets of Fig. 6a should be considered.

First, the dense particle distributions used by Smedley et al. (1999) to make their measurements likely involve a particle-impact resuspension mechanism as well as a mechanism based solely on the applied aerodynamic shear stress. Given a

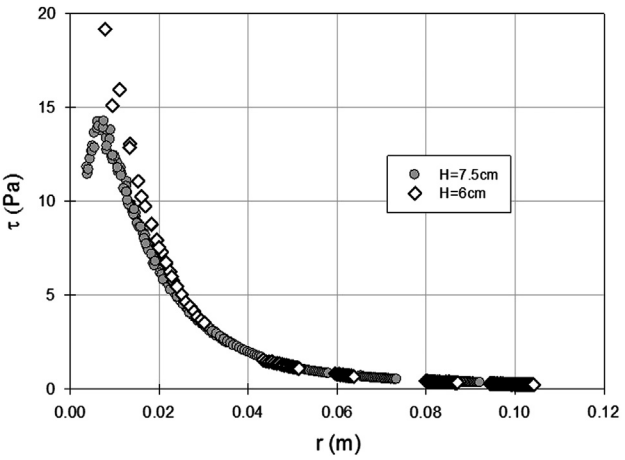

Fig. 4. Shear stress profile for varying standoff distances for subsonic nozzle exit flow. Maximum error caused by impingement location uncertainty and oil viscosity changes due to temperature fluctuations is represented by the size of the symbols.

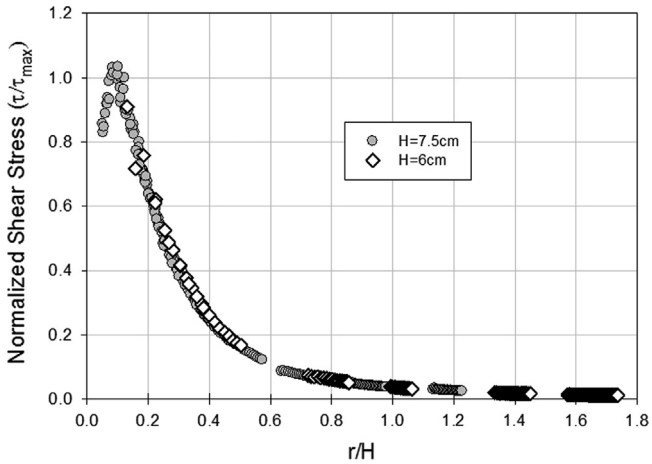

Fig. 5. Normalized shear stress profile for varying standoff distances for subsonic nozzle exit flow.

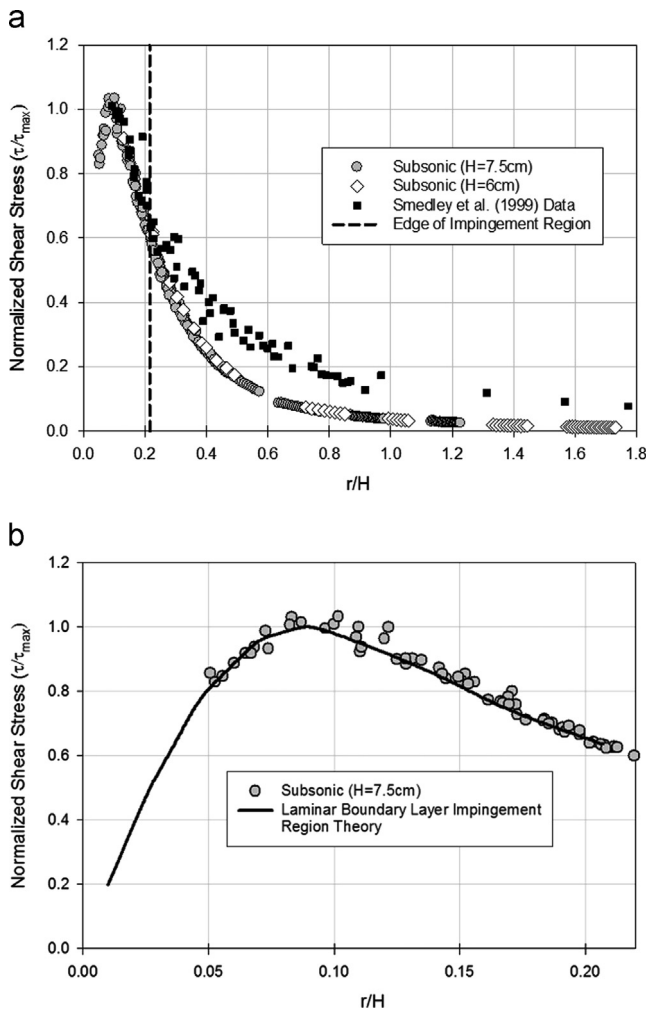

Fig. 6. Present experimental shear stress profile for subsonic flow compared with: (a) data from Smedley et al. (1999) and (b) the predicted shear stress profile based on laminar boundary layer theory for a circular jet within the impingement region.

sufficiently-sparse particle distribution, however, this particle-impact mechanism should become negligible. This suggests that jet-impingement particle-removal experiments with sparse particle distributions are needed, and we have pursued that approach in the next section of this paper.

Second, the present OFI technique for wall shear–stress measurement has no effective frequency response, and thus yields only the mean shear stress. It does not reveal the fluctuating component of wall shear stress beneath a turbulent flow, e. g. due to turbulent bursts as discussed in the Introduction. Consequently, actual particle resuspensions at the larger r/H values in Fig. 6a may not tend toward zero as rapidly as does the mean shear stress that we measured by OFI.

We acquired further OFI data for sonic nozzle-exit conditions at nozzle standoff distances of 12 and 16.5 cm and at a pressure ratio (P_{jet}/P_{atm}) of 2.52 ± 0.04. Fig. 7 shows the shear stress data for the sonic-nozzle-exit experiments, where τ_{max} is now taken directly from the experimental maximum rather than a theoretical maximum, due to the complexity of the flow. (The theoretical solution no longer yields an accurate prediction of maximum shear stress based on initial jet conditions because the flow is not isentropic throughout.)

The sonic data in Fig. 7 show the same normalized shear stress profile as the subsonic data shown earlier. No correction was made to subtract the supersonic region from the jet standoff distance, even though shock diamonds are obviously present. This would not be the expected result, however, if a Laval nozzle was used in place of the present straight tubular nozzle.

3. Particle removal

3.1. Experimental methods

3.1.1. Experimental setup

The present experiments for determining particle removal efficiency used the same glass plate, nozzle, air tank, and regulator as in the OFI experiments just described. The exit pressure ratio, P_{jet}/P_{atm}, was 1.11 ± 0.04 (the same condition as the subsonic OFI tests). For these experiments, however, a pulsed air jet was used instead of a continuous one. A solenoid valve provided consistent jet pulse times of 0.02 s in these experiments.

The OFI data shown previously are steady-state measurements of wall shear stress distributions, since the OFI technique has essentially no frequency response. In order to use these results in understanding particle removal, steady-state removal data are required in principle. This, however, presents a challenge: if a steady jet impingement is applied to a surface with attached particles for an extended time period, all particles will be resuspended and no useful measurement can be made. Instead, it was determined that less than 100% particle removal would be achieved, even at the maximum mean wall shear stress, for air jet impingement under the current conditions (136 m/s nozzle exit speed and 150 mm standoff distance) lasting only 0.02 s. During this interval it is important for steady-state conditions to be reached quickly and maintained, so a fast-acting solenoid valve was used to bring the jet flow up to steady operation in less than 1 ms. Quasi-steady-state flow was verified for at least 18 ms using a fast-response piezoelectric pressure transducer. In that time interval a fluid particle at the nozzle exit velocity would travel almost 20 times the 150 mm standoff distance of the nozzle from the impingement plate.

Under these circumstances we believe that all particle resuspension experiments were performed under quasi-steady-state conditions. We have thus used the measured steady-state OFI wall shear stress distribution to correlate the particle resuspension data.

Relative humidity was recorded for every test, and ranged from 20 to 55%. Within this range, identical experiments were performed at 22% and 52% relative humidity, with no change in resuspension observed.

The particles used in these experiments were Duke Scientific 31-μm-diameter red fluorescent latex microspheres. These particles were deposited on the glass surface using a “settling chamber,” which allowed the particles to separate and settle

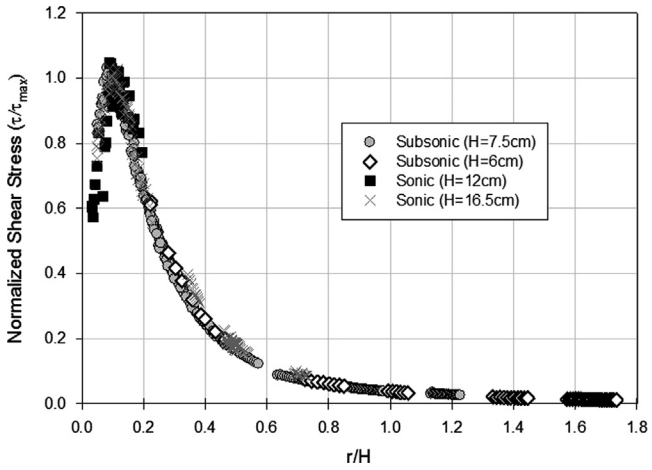

Fig. 7. Normalized shear stress profile for varying standoff distances for subsonic and sonic jet exit flows. All data are normalized by τ_{max}, which is derived theoretically for subsonic exit flow and measured experimentally for sonic exit flow. Maximum error caused by impingement location determination and oil viscosity changes due to temperature fluctuation is represented by the size of the symbols.

in a consistent manner, creating a near-uniform distribution. The particles were distributed in a narrow ~1 cm strip that was aligned perpendicular to the air flow. Only the leading edge of the particle distribution was interrogated, which eliminated the possibility of particles from outside impacting and dislodging particles inside the field-of-view. Static-electric forces between particles and the glass plate were minimized by grounding the plate before and after applying the particles.

Imaging was done with a Photron FASTCAM APX high-speed digital video camera fitted with an Edmund Optics VZM™ 450I microscopic lens with a 3x zoom. The camera frame rate was 10,000 frames per second. It was positioned to image the particles from underneath the glass plate.

3.1.2. Image processing

A routine was written in MATLAB to analyze the resulting particle resuspension images by counting individual particles within a certain field-of-view. This was used to determine the number of particles on the glass surface before and after a 0.02 s air-jet pulse. The routine also calculated the initial mean particle separation for each experiment, this being the average distance between a particle and its closest neighbor. This value is used to determine the effect of particle spacing on removal efficiency.

A particle removal efficiency index was then calculated as

$$Removal\ efficiency = \frac{N_{\text{before}} - N_{\text{after}}}{N_{\text{before}}} \tag{4}$$

The field-of-view for particle counting was chosen to be 6×6 mm, which contained enough particles for a proper statistical sample. A typical 6×6 mm region contained 75 particles in these experiments.

3.2. Experimental results

As discussed earlier, we were primarily interested in the effect of particle spacing (i.e. the density of the applied particle distribution on the test surface) on jet-impingement-induced particle resuspension. Thus the mean particle spacing was calculated for every test. Results yielded an overall average spacing of 13.37 particle diameters (415 μm) with a standard deviation of 2.68 particle diameters.

In order to determine the effect of particle spacing on resuspension, several tests were performed at jet-impingement location $r/H = 0.5$ while varying the mean particle spacing from about 5.6 to 21 particle diameters (174–651 μm). Fig. 8 shows these results in terms of particle removal efficiency vs. mean particle spacing. For a particle spacing of 10 diameters and greater, the removal efficiency becomes effectively constant in Fig. 8, i.e. it becomes effectively independent of particle spacing for such "sparse" particle distributions. This trend is consistent for each data set taken at any radial distance from the jet impingement point.

For particle spacing less than 10 particle diameters in Fig. 8, the removal efficiency is a strong function of spacing. Here the distribution is "dense," although we note an important difference with dense-distribution results in the literature, described earlier, where particle impacts play a commanding role. Here, despite the dense distribution, resuspension by particle impact has been essentially eliminated in the design of the experiment. This is an unknown regime of particle removal, and its proper investigation is unfortunately beyond the present scope.

Further data were taken at various r/H values for jet impingement with the nozzle height set at 15 cm ($H/D = 40$). The radial distance was varied by re-positioning the nozzle along a radius while keeping the camera focused on a single 6×6 mm region of the glass surface. The resulting data, shown in Fig. 9, give particle removal efficiency as a function of normalized radius r/H from the jet impingement point.

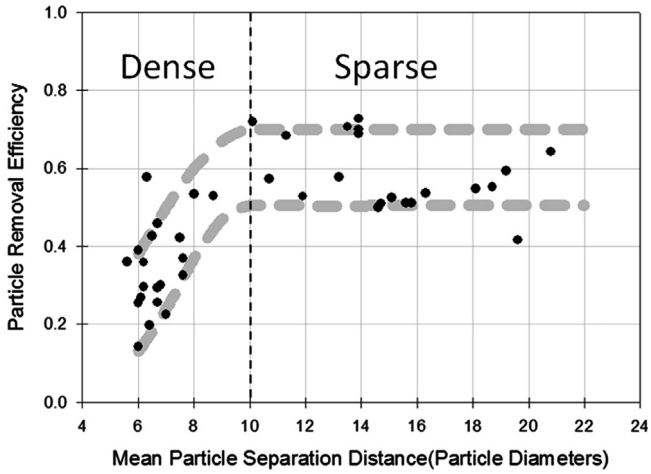

Fig. 8. Removal efficiency vs. mean particle separation for $r = 75$ mm and $H = 150$ mm ($r/H = 0.5$). For a separation greater than 10 particle diameters, removal efficiency becomes independent of particle separation distance.

Fig. 9 reveals that the maximum particle removal efficiency occurs around $r/H=0.1$. This location is near the location of maximum shear stress according to the OFI results shown earlier. The error bars shown in r/H are due to the 6-mm width of the viewing field, while the error in removal efficiency is represented as one standard deviation of each data set. The data in Fig. 9 consist of twenty repeated experiments performed at r/H values of 0.2 and 0.5, and ten repeats performed at all other radial distances. The standard deviation and mean removal efficiency were not affected when 10 additional tests were performed beyond the initial 10 at $r/H=0.2$ and 0.5. Therefore it was concluded that ten tests at each radial location were sufficient for meaningful statistics.

Using the experimental OFI data presented earlier, the aerodynamic shear stress at each r/H location tested in Fig. 9 can be determined from the known jet standoff distance, radial distance from the impingement point, jet exit velocity, and nozzle diameter. This was done using subsonic-jet-exit data only, and the results were combined with those of Fig. 9 to produce Fig. 10, which shows particle removal efficiency as a function of the non-dimensional shear stress applied by the impinging jet.

The error bars in shear stress in Fig. 10 are derived from the experimental results of Fig. 5. The width of the field-of-view in the particle removal experiments is 6 mm, which corresponds to an error in r/H of ± 0.02 for a jet standoff distance of 150 mm. The shear stress varies with r/H, and because r/H varies in each particle removal test due to the width of the field-of-view, the shear stress also varies from one side of the field-of-view to the other. Thus the range of shear stress for each r/H location yields the corresponding error bar shown in Fig. 10. Additional data were taken at a nozzle standoff distance of 105 mm, where the removal efficiency is found to follow the same trend as the data of Fig. 10 with a standoff distance of 150 mm.

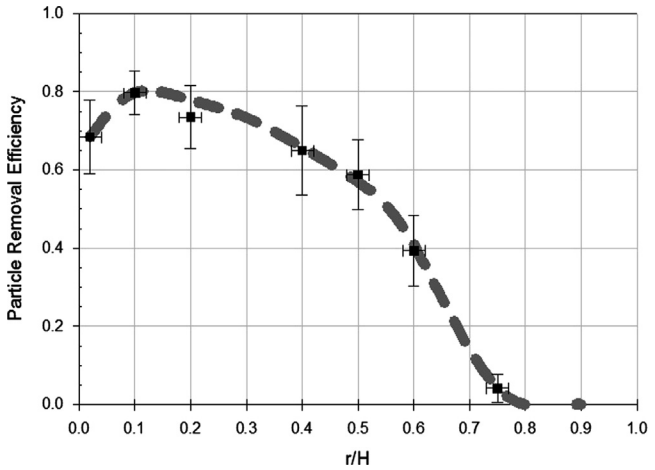

Fig. 9. Sparse-distribution particle removal efficiency for various radial distances from the jet impingement point at a nozzle standoff distance of 150 mm. The jet pressure ratio was $P_{jet}/P_{atm}=1.11$, with a jet duration of 0.02 s. Vertical error bars represent the standard deviation of the mean. Horizontal error bars correspond to the 6 mm width of the viewing field.

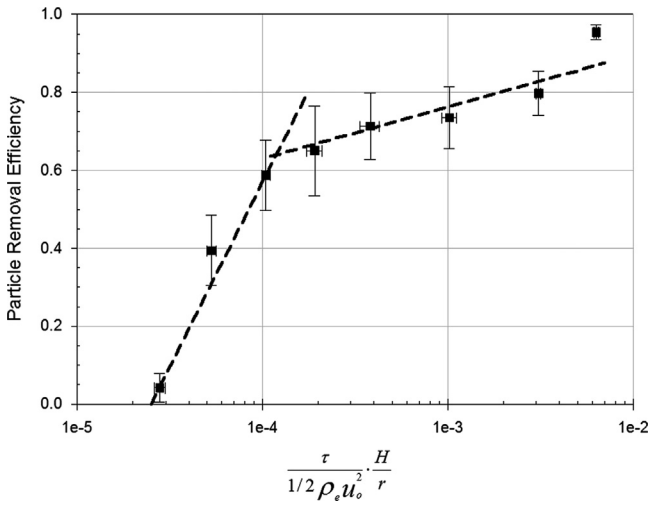

Fig. 10. Particle removal efficiency vs. nondimensionalized shear stress. Data were taken for a sparse distribution (mean particle separation greater than 10 particle diameters). Vertical error bars represent the standard deviation of the average removal efficiency and horizontal error bars represent the change in shear stress based on the 6 mm width of the viewing field.

The results of Fig. 10 show a sharp change in the trend of particle removal efficiency at a non-dimensionalized wall shear stress value of about 10^{-4}. Below this value – in the far field of the jet-impingement phenomenon – the aerodynamic shear stress is marginal or too low to cause significant removal of the present particles from the present substrate. However, above a non-dimensionalized wall shear stress value of about 10^{-4} – in the near field of the jet-impingement phenomenon – Fig. 10 shows a consistent trend of particle removal efficiency in the 60–90% range.

For this experiment, then, we can define a critical shear stress level (τ_{cr}) of about 1 Pa, based on the observed non-dimensionalized shear stress value of about 10^{-4}. Using the jet-impingement shear–stress data of Fig. 4 as an example, the critical value of shear stress for particle removal occurs at a radius of 0.05–0.06 m. This is the effective radius of particle removal for the present test conditions, since outside this radius τ is less than τ_{cr}, so few particles are removed as a result of the jet impingement airflow. For many practical applications of particle resuspension from surfaces by gas-jet impingement, it is important to have such a criterion for the effective radius of the process.

4. Conclusions

The mean shear stress profile of a round turbulent air jet impinging normally upon a surface has been determined using oil-film interferometry. Experiments were performed for subsonic nozzle exit flows, where $P_{jet}/P_{atm}=1.11\pm0.04$, with jet standoff distances of 0.06 m and 0.075 m, and for sonic exit flows, where $P_{jet}/P_{atm}=2.52\pm0.04$, with jet standoff distances of 0.12 m and 0.165 m. When the resulting data were normalized in terms of r/H (radial distance from the jet impingement point divided by the jet standoff distance) and τ/τ_{max}, all four cases yielded very comparable results. These experiments show that a shear stress maximum occurs at a normalized radial distance from the jet impingement point, r/H, of about 0.09.

These results were compared with those of Smedley et al. (1999), who inferred wall shear stress from particle-removal experiments. The two data sets are similar, but they differ especially at larger values of r/H. This raises questions about particle resuspension by air-jet impingement in dense versus sparse particle distributions.

Further experiments considered the resuspension of 31 μm-diameter latex microspheres from a flat glass substrate using the same impinging round turbulent jet flow that yielded the above shear stress results. First, widely-differing particle densities on the glass substrate were tested at one jet impingement condition. This revealed that the particle removal efficiency of the impinging jet flow can only be considered independent of particle distribution density when the mean distance between particles is at least 10 particle diameters. We refer to such a condition as a “sparse” particle distribution. Only sparse particle distributions were used in the remainder of the study.

Further experiments then measured the particle removal efficiency as a function of local mean shear stress produced by the impinging-jet flowfield. This revealed that there is a value of non-dimensionalized shear stress, approximately 10^{-4}, below which few particles are removed from the substrate. For given jet conditions, a corresponding critical shear stress (τ_{cr}) can be derived, which for our experiments is about 1 Pa. Where τ is greater than τ_{cr}, consistent particle removal efficiencies in the 60–95% range are observed. We conclude that τ_{cr} can be used to define the effective radius of particle removal due to round turbulent air jet impingement on a planar surface.

References

Braaten, D.A., Shaw, R.H., & Paw, U.K.T. (1990). Particle resuspension in a turbulent boundary layer. *Journal of Aerosol Science*, *21*, 613–628.

Braaten, D.A. (1994). Wind-tunnel experiments of large particle reentrainment-deposition and development of large particle scaling parameters. *Aerosol Science and Technology*, *21*(2), 157–169.

Corino, E.R., & Brodkey, R.S. (1969). A visual investigation of the wall region in a turbulent flow. *Journal of Fluid Mechanics*, *37*(part 1), 1–30.

Driver, D.M. (2003). Application of oil-film interferometry skin-friction measurement to large wind tunnels. *Experiments in Fluids*, *34*, 717–725.

Fromentin, A. (1989). Time dependent particle resuspension from a multi-layer deposit by turbulent flow. *Journal of Aerosol Science*, *20*, 911–914.

Ibrahim, A.H., Dunn, P.F., & Brach, R.M. (2003). Microparticle detachment from surfaces exposed to turbulent air flow: controlled experiments and modeling. *Journal of Aerosol Science*, *34*(6), 765–782.

Ibrahim, A.H., Dunn, P.F., & Brach, R.M. (2004). Microparticle detachment from surfaces exposed to turbulent air flow: effects of flow and particle deposition characteristics. *Journal of Aerosol Science*, *35*(7), 805–821.

Ibrahim, A.H., & Dunn, P.F. (2006). Effects of temporal flow acceleration on the detachment of microparticles from surfaces. *Journal of Aerosol Science*, *37*(10), 1258–1266.

Ibrahim, A.H., Dunn, P.F., & Qazi, M.F. (2008). Experiments and validation of a model for microparticle detachment from a surface by turbulent air flow. *Journal of Aerosol Science*, *39*(8), 645–656.

John, W., Fritter, D.N., & Winklmayr, W. (1991). Resuspension Induced by impacting particles. *Journal of Aerosol Science*, *22*(6), 723–736.

Naughton, J.W. (2005). High-quality skin friction measurements in 2-D flows using oil film interferometry. In: Proceedings of the Twenty first International Congress on Instrumentation in Aerospace Simulation Facilities, 2005. V. 166–175.

Naughton, J.W., & Lin, T. (2007). Photogrammetry in Oil-Film Interferometry. *AIAA Journal*, *45*(7), 1620–1629.

Nicholson, K.W. (1988). A review of particle resuspension. *Atmospheric Environment*, *22*, 2639–2651.

Phares, D.J., Smedley, G.T., & Flagan, R.C. (2000). The wall shear stress produced by the normal impingement of a jet on a flat surface. *Journal Fluid Mechanics*, *418*, 351–375.

Pope, S.B. (2000). *Turbulent Flows*. Cambridge University Press: Cambridge.

Reeks, M.W., Reed, J., & Hall, D. (1988). On the resuspension of small particles by a turbulent flow. *Journal of Physics D:Applied Physics*, *21*(4), 574–589.

Reeks, M.W., & Hall, D. (2001). Kinetic models for particle resuspension in turbulent flows: theory and measurement. *Journal of Aerosol Science*, *32*(1), 1–31.

Smedley, G.T., Phares, D.J., & Flagan, R.C. (1999). Entrainment of fine particles from surfaces by gas jets impinging at a normal incidence. *Experiments in Fluids*, *26*(4), 324–334.

Smedley, G.T., Phares, D.J., & Flagan, R.C. (2001). Entrainment of fine particles from surfaces by gas jets impinging at oblique incidence. *Experiments in Fluids*, *30*(2), 135–142.

Tanner, L.H., & Blows, L.G. (1976). A study of the motion of oil films on surfaces in air flow, with the application to measurement of skin friction. *Journal of Physics E*, *9*(3), 194–202.
Ziskind, G., Fichman, M., & Gutfinger, C. (1995). Resuspension of particulates from surfaces to turbulent flows: review and analysis. *Journal of Aerosol Science*, *26*(4), 613–644.
Ziskind, G., Fichman, M., & Gutfinger, C. (1997). Adhesion moment model for estimating particle detachment from a surface. *Journal of Aerosol Science*, *28*(4), 623–634.
Ziskind, G., Yarin, L.P., Peles, S., & Gutfinger, C. (2002). Experimental investigation of particle removal from surfaces by pulsed air jets. *Aerosol Science & Technology*, *36*(5), 652–659.
Ziskind, G. (2006). Particle resuspension from surfaces: revisited and re-evaluated. *Reviews in Chemical Engineering*, *22*(1-2), 1–123.